Solid Solutions $RE_{16}Rh_{11-x}Z_x$ (RE = La, Ce, Pr, Nd, Sm; Z = Ga, Zn, Cd, In, Sn, Sb, Pb, Bi) – Centrosymmetric $n = 2$ Variants of Parthé's Homologous Series $A_{5n+6}B_{3n+5}$

Frank Tappe, Falko M. Schappacher, Thorsten Langer, Inga Schellenberg, and Rainer Pöttgen

Institut für Anorganische und Analytische Chemie, Universität Münster, Corrensstrasse 30, D-48149 Münster, Germany

Reprint requests to R. Pöttgen. E-mail: pottgen@uni-muenster.de

Z. Naturforsch. **2012**, *67b*, 594 – 604 / DOI: 10.5560/ZNB.2012-0070
Received March 7, 2012

Dedicated to Professor Wolfgang Beck on the occasion of his 80th birthday

Several samples of solid solutions $RE_{16}Rh_{11-x}Z_x$ (RE = La, Ce, Pr, Nd, Sm; Z = Ga, Zn, Cd, In, Sn, Sb, Pb, Bi) were synthesized by high-frequency melting of the elements in sealed tantalum ampoules. The samples were characterized by powder X-ray diffraction, and the structures of eight compounds were refined on the basis of single-crystal X-ray diffractometer data. The compounds crystallize with a centrosymmetric variant (space group $P4/mbm$) of the $Ca_{16}Sb_{11}$ type ($P\bar{4}2_1m$). The relation between both structure types is discussed on the basis of a group-subgroup scheme. Only for $La_{16}Rh_8Sn_3$ we observed full rhodium-tin ordering. The striking structural motif is a chain of face-sharing square prisms (filled with tin) and anti-prisms (filled with rhodium). The $La_{16}Rh_8Sn_3$ structure is closely related to the structure types W_5Si_3, $Ca_{16}Sb_{11}$, Y_3Rh_2, $Sm_{26}Co_{11}Ga_6$, $Pu_{31}Pt_{20}$, and $Yb_{36}Sn_{23}$ and is the centrosymmetric $n = 2$ member of Parthé's $A_{5n+6}B_{3n+5}$ series. ^{119}Sn Mössbauer spectra resolved the two crystallographically independent tin sites of $La_{16}Rh_8Sn_3$, while a $Pr_{16}Rh_9Sb_2$ sample shows only a singlet in its ^{121}Sb Mössbauer spectrum.

Key words: Intermetallics, Rhodium, Solid Solutions

Introduction

The cerium-rich part of the Ce-Rh system [1] is characterized by different structure types with common basic building units, *i. e.* rhodium-centered trigonal prisms of cerium. These $RhCe_6$ units occur in the structures of Ce_7Rh_3 [1, 2], Ce_5Rh_3 [1], Ce_5Rh_4 [3], and CeRh [4], and they are preserved also in ternary cerium-rich compounds of the Ce-Rh-Cd system, explicitly Ce_2Rh_2Cd [5], $Ce_{15}Rh_5Cd_2$ [6], Ce_4RhCd [7], and $Ce_{23}Rh_7Cd_4$ [8]. The latter three structures can be considered as intergrowth variants. Looking at the compositions Ce_4RhCd (*i. e.* $Ce_{16}Rh_4Cd_4$), $Ce_{23}Rh_7Cd_4$, and $Ce_{15}Rh_5Cd_2$ (*i. e.* $Ce_{30}Rh_{10}Cd_4$), one formally adds a formula unit Ce_7Rh_3 in each step [9], and all rhodium atoms keep the trigonal prismatic cerium coordination. Thus, parts of the binary Ce_7Rh_3 structure are preserved in the ternary cadmium intermetallics.

During recent crystal growth experiments of the ternary phase $Ce_{15}Rh_5Cd_2$ [6], we obtained small amounts of a well crystallized by-product. The tetragonal primitive unit cell with $a = 1189.7$ and $c = 985.1$ pm and the initially refined composition '$Ce_{16}Rh_{11}$' obtained from the single-crystal X-ray data pointed to the tetragonal $Ca_{16}Sb_{11}$-type [10] structure. However, the Ce-Rh phase diagram [1] does not contain such a phase, and an EDX analyses of the investigated crystals showed approximately 5 % cadmium content, pointing to a solid solution $Ce_{16}Rh_{11-x}Cd_x$. Subsequent more detailed phase-analytical studies of the *RE*-*T*-Cd systems revealed that such ternary phases also exist with other rare earth elements, and that the cadmium sites can be substituted.

Herein we report on diverse solid solutions $RE_{16}Rh_{11-x}Z_x$ (RE = La, Ce, Pr, Nd, Sm; Z = Ga, Zn, Cd, In, Sn, Sb, Pb, Bi) and the fully ordered stannide $La_{16}Rh_8Sn_3$. These compounds are the missing

centrosymmetric $n = 2$ variants of Parthé's homologous series $A_{5n+6}B_{3n+5}$ [11]. Besides extended structural work we studied selected samples by ^{119}Sn and ^{121}Sb Mössbauer spectroscopy.

Experimental

Synthesis

Starting materials for the preparation of samples of the solid solutions $RE_{16}Rh_{11-x}Z_x$ were ingots of the rare earth elements (Johnson Matthey or smart elements), rhodium powder (Heraeus), zinc granules (Merck), gallium lumps (Johnson Matthey), a cadmium rod (Johnson Matthey), indium tear drops (Johnson Matthey), tin granules (Merck), antimony shots (ABCR GmbH), a lead rod (Johnson Matthey), and bismuth granules (Chempur), all with stated purities better than 99.9 %. The larger lanthanum, cerium, praseodymium, neodymium, and samarium ingots were cut into smaller pieces under dried (Na wire) paraffin oil, washed with dried *n*-hexane (Na wire) and kept in Schlenk tubes prior to the reactions. The elements were then weighed in the appropiate amounts listed in Table 1 and arc-welded [12] in small tantalum ampoules under an argon atmosphere of *ca.* 800 mbar. The argon was purified with titanium sponge (900 K), silica gel, and molecular sieves. The ampoules were subsequently placed in the water-cooled sample chamber of an induction furnace [13] (Hüttinger Elektronik, Freiburg, Germany, Typ TIG 2.5/300), rapidly heated to 1470 K and kept at that temperature for 5 min. The tubes were then rapidly cooled to 920 K and annealed at that temperature for another three h, followed by quenching by switching off the power supply. The temperature was controlled by a Sensor Therm Methis MS09 pyrometer with an accuracy of ±30 K. The brittle polycrystalline $RE_{16}Rh_{11-x}Z_x$ samples could easily be separated from the tantalum containers. No reactions with the crucible material were observed. The $RE_{16}Rh_{11-x}Z_x$ samples are sensitive to moisture.

The samples used for crystal growth have been annealed differently. The sealed tantalum ampoules were sealed in evacuated quartz tubes for oxidation protection and heated within 4 h to 1470 K in a muffle furnace. The tubes were kept at that temperature for 8 h, then cooled to 870 K at a rate of 3 K h^{-1}, kept there for another 4 d and then cooled to room temperature by radiative heat loss.

EDX data

The $RE_{16}Rh_{11-x}Z_x$ single crystals studied on the diffractometers were investigated by semiquantitative EDX analyses by use of a Zeiss EVO MA10 scanning electron microscope (variable pressure mode) with LaF_3, CeO_2, PrF_3, NdF_3, Rh, and Cd as standards. The experimentally observed compositions were close to the ideal ones. No impurity elements were found.

Table 1. Lattice parameters of samples from diverse solid solutions $RE_{16}Rh_{11-x}Z_x$.

Compound	*a* (pm)	*c* (pm)	*V* (nm^3)
$La_{16}Rh_9Zn_2$	1195.2(1)	1004.3(1)	1.4346
$Pr_{16}Rh_9Zn_2$	1179.9(4)	990.3(6)	1.3787
$Pr_{16}Rh_{9.18(4)}Zn_{1.82(4)}$ [a]	1173.1(2)	986.2(2)	1.3572
$La_{16}Rh_9Ga_2$	1194.3(1)	1002.0(1)	1.4292
$La_{16}Rh_9Cd_2$	1201.0(1)	1006.9(2)	1.4523
$Ce_{16}Rh_9Cd_2$	1182.2(1)	987.4(2)	1.3800
$Ce_{16}Rh_{10.32(10)}Cd_{0.68(10)}$ [a]	1189.7(2)	985.1(2)	1.3943
$Pr_{16}Rh_9Cd_2$	1181.7(2)	987.0(2)	1.3783
$Sm_{16}Rh_9Cd_2$	1169.0(4)	977.6(3)	1.3360
$La_{16}Rh_9In_2$	1205.8(2)	1005.1(3)	1.4614
$Pr_{16}Rh_9In_2$	1185.9(2)	984.9(4)	1.3851
$Pr_{16}Rh_{9.55(9)}In_{1.45(9)}$ [a]	1185.7(2)	985.5(2)	1.3855
$Nd_{16}Rh_9In_2$	1180.1(4)	981.4(3)	1.3667
$Nd_{16}Rh_{9.61(7)}In_{1.39(7)}$ [a]	1173.4(2)	981.4(2)	1.3513
$La_{16}Rh_{10}Sn$	1204.0(3)	1009.2(6)	1.4629
$La_{16}Rh_9Sn_2$	1208.7(1)	1002.1(2)	1.4640
$La_{16}Rh_{8.5}Sn_{2.5}$	1214.2(1)	997.6(2)	1.4707
$La_{16}Rh_8Sn_3$	1220.7(1)	997.9(2)	1.4870
$La_{16}Rh_8Sn_3$ [a]	1222.0(2)	998.9(2)	1.4916
$La_{16}Rh_7Sn_4$	1221.4(3)	996.7(3)	1.4869
$Ce_{16}Rh_9Sn_2$	1205.6(3)	979.6(3)	1.4238
$Pr_{16}Rh_9Sn_2$	1192.1(3)	979.3(2)	1.3917
$Pr_{16}Rh_{9.38(10)}Sn_{1.62(10)}$ [a]	1189.63(7)	979.9(1)	1.3868
$Pr_{16}Rh_9Sb_2$	1175.9(4)	986.7(4)	1.3644
$Pr_{16}Rh_{10.20(9)}Sb_{0.80(9)}$ [a]	1163.25(7)	988.2(1)	1.3372
$La_{16}Rh_9Pb_2$	1211.6(1)	1007.6(2)	1.4791
$La_{16}Rh_8Pb_3$	1218.6(2)	1004.7(3)	1.4920
$La_{16}Rh_{8.76(2)}Pb_{2.24(2)}$ [a]	1220.3(2)	1007.7(2)	1.5006
$Ce_{16}Rh_9Pb_2$	1197.1(2)	978.9(2)	1.4028
$Pr_{16}Rh_9Pb_2$	1187.8(1)	983.7(2)	1.3879
$Nd_{16}Rh_9Pb_2$	1184.2(2)	983.3(3)	1.3789
$La_{16}Rh_9Bi_2$	1204.0(3)	1007.2(3)	1.4601

[a] Single-crystal data.

X-Ray diffraction

All polycrystalline $RE_{16}Rh_{11-x}Z_x$ samples were characterized by powder X-ray diffraction: Guinier camera (imaging plate detector, Fujifilm BAS-1800 readout system), Cu $K_{\alpha 1}$ radiation and α-quartz ($a = 491.30$ and $c = 540.46$ pm) as the internal standard. The tetragonal lattice parameters (Table 1) resulted from least-squares refinements of the powder diffraction data. The correct indexing was ensured with the help of intensity calculations [14].

Small single crystals were selected from eight $RE_{16}Rh_{11-x}Z_x$ samples. The crystals were obtained from the crushed samples prepared by the long annealing sequences in the muffle furnace. The quality of the crystals was first checked by Laue photographs on

Table 2. Crystal data and structure refinement for $Pr_{16}Rh_{9.18}Zn_{1.82}$, $Ce_{16}Rh_{10.32}Cd_{0.68}$, $Pr_{16}Rh_{9.55}In_{1.45}$, and $Nd_{16}Rh_{9.61}In_{1.39}$; space group $P4/mbm$, $Z = 2$.

Empirical formula	$Pr_{16}Rh_{9.18}Zn_{1.82}$	$Ce_{16}Rh_{10.32}Cd_{0.68}$	$Pr_{16}Rh_{9.55}In_{1.45}$	$Nd_{16}Rh_{9.61}In_{1.39}$
Molar mass, g mol^{-1}	3318.25	3380.34	3403.84	3456.41
Unit cell dimensions	Table 1	Table 1	Table 1	Table 1
Calculated density, g cm^{-3}	8.12	8.05	8.16	8.50
Crystal size, μm^3	$20 \times 20 \times 30$	$20 \times 20 \times 40$	$10 \times 20 \times 40$	$10 \times 20 \times 30$
Detector distance, mm	80	90	80	80
Exposure time, min	6	6	5	6
ω range; increment, deg.	0 – 180; 1.0	0 – 180; 1.0	0 – 180; 1.0	0 – 180; 1.0
Integr. param. A, B, EMS	12.0, 2.5, 0.012	12.0, 3.0, 0.012	12.5, 3.0, 0.012	13.0, 3.5, 0.012
Transm. ratio (max/min)	0.634/0.347	0.566/0.340	0.582/0.218	0.551/0.253
Absorption coefficient, mm^{-1}	35.0	31.9	34.2	36.9
F(000), e	2823	2850	2890	2921
θ range, deg.	2 – 30	2 – 30	2 – 30	2 – 30
Range in *hkl*	$-14/16, \pm16, \pm13$	$\pm16, \pm16, \pm13$	$\pm16, \pm16, \pm13$	$\pm16, \pm16, \pm13$
Total no. reflections	13527	14398	9947	13270
Independent reflections/R_{int}	1118/0.063	1145/0.125	1117/0.097	1110/0.077
Reflections with $I > 2\sigma\ (I)/R_\sigma$	866/0.045	488/0.188	869/0.055	894/0.044
Data/parameters	1118/46	1145/46	1117/46	1110/46
Goodness-of-fit on F^2	0.945	0.405	1.066	1.012
$R1/wR2$ for $[I > 2\sigma(I)]$	0.030/0.035	0.022/0.031	0.043/0.052	0.037/0.035
$R1/wR2$ for all data	0.057/0.039	0.081/0.037	0.069/0.056	0.059/0.038
Extinction coefficient	0.00007(2)	0.000307(14)	0.00020(2)	0.000096(16)
Largest diff. peak/hole, e Å^{-3}	$1.99/-2.35$	$1.70/-1.73$	$2.27/-2.26$	$2.55/-1.91$

a Buerger camera (white Mo radiation). Most intensity data were collected at room temperature by use of a Stoe IPDS-II imaging plate diffractometer in oscillation mode (graphite-monochromatized Mo K_α radiation). Two of the crystals were measured on a Nonius CAD4 four-circle diffractometer with graphite-monochromatized Mo K_α radiation ($\lambda = 71.073$ pm for $La_{16}Rh_{8.75}Pb_{2.25}$) and Ag K_α ($\lambda = 56.086$ pm for $Pr_{16}Rh_{10.20}Sb_{0.80}$) radiation and a scintillation counter with pulse-height discrimination. Scans were taken in the $\omega/2\theta$ mode. Numerical absorption corrections were applied to all data sets. The relevant details concerning the data collections and evaluations are listed in Tables 2 and 3.

Structure refinements

All data sets showed primitive tetragonal lattices with high Laue symmetry, and the systematic extinctions were compatible with the centrosymmetric space group $P4/mbm$. The starting atomic parameters were determined *via* Direct Methods with SHELXS-97 [15], and the structures were refined using SHELXL-97 [16] (full-matrix least-squares on F^2) with anisotropic atomic displacement parameters for all sites. As a check for the correct composition, all occupancy parameters were refined in a separate series of least-squares cycles. All rare earth sites were fully occupied within two standard deviations and, except for $La_{16}Rh_8Sn_3$, where two of the five crystallographically independent rhodium sites showed mixed occupancy with the Z component, leading to the compositions listed in Tables 2 and 3. For the pairs Rh/Cd, Rh/In, Rh/Sb, and Rh/Sn the small differences in scattering power led to higher standard deviations for the occupancy parameters. For the two mixed-occupied sites we observed slightly enhanced displacement parameters, a consequence of the difference in size between the rhodium atoms and the different Z components. In the final cycles, these mixed occupancies were refined as least-squares variables. The final difference Fourier syntheses were flat (Tables 2 and 3). The positional parameters and interatomic distances (exemplarily for $La_{16}Rh_8Sn_3$) are listed in Tables 4 and 5.

Further details of the crystal structure investigation may be obtained from Fachinformationszentrum Karlsruhe, 76344 Eggenstein-Leopoldshafen, Germany (fax: +49-7247-808-666; e-mail: crysdata@fiz-karlsruhe.de, http://www.fiz-karlsruhe.de/request_for_deposited_data.html) on quoting the deposition number CSD-424338 ($Pr_{16}Rh_{9.18}Zn_{1.82}$), CSD-424334 ($Ce_{16}Rh_{10.32}Cd_{0.68}$), CSD-424335 ($Pr_{16}Rh_{9.55}In_{1.45}$), CSD-424337 ($Nd_{16}Rh_{9.61}In_{1.39}$), CSD-424333 ($La_{16}Rh_8Sn_3$), CSD-424340 ($Pr_{16}Rh_{9.38}Sn_{1.62}$), CSD-424339 ($Pr_{16}Rh_{10.20}Sb_{0.80}$), and CSD-424336 ($La_{16}Rh_{8.76}Pb_{2.24}$).

Mössbauer spectroscopy

A $Ca^{119m}SnO_3$ and a $Ba^{121m}SnO_3$ source were used for the Mössbauer spectroscopic experiments. The measure-

Table 3. Crystal data and structure refinement for $La_{16}Rh_8Sn_3$, $Pr_{16}Rh_{9.38}Sn_{1.62}$, $Pr_{16}Rh_{10.20}Sb_{0.80}$, and $La_{16}Rh_{8.76}Pb_{2.24}$, space group $P4/mbm$, $Z = 2$.

Empirical formula	$La_{16}Rh_8Sn_3$	$Pr_{16}Rh_{9.38}Sn_{1.62}$	$Pr_{16}Rh_{10.20}Sb_{0.80}$	$La_{16}Rh_{8.76}Pb_{2.24}$
Molar mass, g mol^{-1}	3401.91	3412.13	3401.64	3588.68
Unit cell dimensions	Table 1	Table 1	Table 1	Table 1
Calculated density, g cm^{-3}	7.57	8.17	8.45	7.94
Crystal size, μm^3	$20 \times 20 \times 40$	$20 \times 20 \times 30$	$20 \times 20 \times 20$	$10 \times 10 \times 20$
Detector distance, mm	90	–	–	90
Exposure time, min	6	–	–	6
ω range; increment, deg.	0 – 180; 1.0	–	–	0 – 180; 1.0
Integr. param. A, B, EMS	12.8, 3.0, 0.011	–	–	12.8, 2.8, 0.012
Transm. ratio (max/min)	0.638/0.356	0.479/0.378	0.632/0.570	0.600/0.372
Absorption coefficient, mm^{-1}	29.0	34.3	18.7 (Ag radiation)	39.4
F(000), e	2844	2894	2888	2980
θ range, deg.	2 – 30	2 – 30	3 – 26	2 – 30
Range in hkl	$\pm17, \pm17, \pm14$	$\pm16, \pm16, -13/11$	$\pm18, \pm18, -15/1$	$\pm17, \pm17, \pm14$
Total no. reflections	15505	15170	10848	15059
Independent reflections/R_{int}	1219/0.175	1141/0.274	1483/0.357	1229/0.163
Reflections with $I > 2\sigma\ (I)/R_\sigma$	543/0.219	799/0.079	679/0.151	748/0.122
Data/parameters	1219/44	1141/46	1483/45	1229/46
Goodness-of-fit on F^2	0.535	1.078	0.986	0.883
$R1/wR2$ for $[I > 2\sigma\ (I)]$	0.032/0.034	0.043/0.093	0.053/0.071	0.053/0.049
$R1/wR2$ for all data	0.141/0.057	0.079/0.111	0.171/0.100	0.117/0.058
Extinction coefficient	0.000112(16)	0.00003(4)	–	0.000002(15)
Largest diff. peak/hole, e Å^{-3}	2.17/ – 1.86	5.96/ – 3.01	4.21/ – 5.07	3.85/ – 2.64

ments were carried out in a nitrogen bath cryostat at 77 K. The Mössbauer sources were kept at room temperature. The samples were enclosed in small PMMA containers at a thickness corresponding to about 10 mg of the Mössbauer-active element per cm^2.

Discussion

Crystal chemistry

Several new $RE_{16}Rh_{11-x}Z_x$ (RE = La, Ce, Pr, Nd, Sm; Z = Ga, Zn, Cd, In, Sn, Sb, Pb, Bi) samples (Table 1) with a tetragonal structure have been prepared. They derive from the structure type $Ca_{16}Sb_{11}$ [10]. The lattice parameters of our samples depend on the size of the respective rare earth element and the Z component as well. The eight structure refinements clearly showed that two Wyckoff sites are either fully occupied by tin (in $La_{16}Rh_8Sn_3$) or reveal mixed occupancies. As an example we studied the homogeneity range for $La_{16}Rh_{11-x}Sn_x$ in more detail. The course of the lattice parameters within the solid solution is shown in Fig. 1. We observe an anisotropic behavior, *i. e.* an increase of the a and a decrease of the c parameter. At $x \approx 4$ we reach the limit of the solid solution. The powder patterns of such a sample already showed by-products.

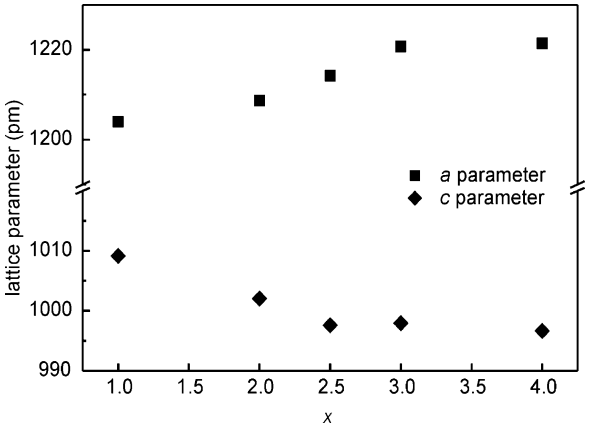

Fig. 1. Course of the cell parameters in the solid solution $La_{16}Rh_{11-x}Sn_x$.

The small Z content in many of our samples suggested the possibility of binary rare earth-rhodium intermetallics. We tried the intended 16-11 compositions with lanthanum and cerium, however, only the known binaries [1, 17] resulted from these experiments. The Z component is required for the stabilization of our phases.

Since $La_{16}Rh_8Sn_3$ was obtained as a ternary, fully ordered compound, in the following discussion we fo-

Table 4. Atomic coordinates and isotropic displacement parameters of several $RE_{16}Rh_{11-x}Z_x$ compounds; space group $P4/mbm$.

Atom	Wyckoff site	x	y	z	U_{eq}
$Pr_{16}Rh_{9.18(4)}Zn_{1.82(4)}$					
Pr1	16*l*	0.08039(4)	0.20277(4)	0.31145(4)	149(1)
Pr2	8*i*	0.21166(6)	0.07186(6)	0	223(2)
Pr3	4*h*	0.14366(5)	$x+1/2$	1/2	159(2)
Pr4	4*f*	0	1/2	0.20198(8)	171(2)
Rh1	8*k*	0.17666(6)	$x+1/2$	0.22321(9)	214(2)
Rh2	4*h*	0.60376(9)	$x+1/2$	1/2	207(3)
Rh3	4*e*	0	0	0.15570(13)	185(2)
58(3) % Zn1	4*g*	0.65981(13)	$x+1/2$	0	366(9)
42(3) % Rh4					
65(4) % Zn2	2*b*	0	0	1/2	224(10)
35(4) % Rh5					
$Ce_{16}Rh_{10.32(10)}Cd_{0.68(10)}$					
Ce1	16*l*	0.07956(5)	0.20516(5)	0.30991(6)	153(1)
Ce2	8*i*	0.20919(10)	0.07559(10)	0	244(2)
Ce3	4*h*	0.14588(8)	$x+1/2$	1/2	152(3)
Ce4	4*f*	0	1/2	0.21063(13)	169(3)
Rh1	8*k*	0.17721(8)	$x+1/2$	0.22749(14)	239(3)
Rh2	4*h*	0.59918(12)	$x+1/2$	1/2	196(4)
Rh3	4*e*	0	0	0.1543(2)	199(4)
25(9) % Cd1	4*g*	0.65981(12)	$x+1/2$	0	213(7)
75(9) % Rh4					
18(12) % Cd2	2*b*	0	0	1/2	177(9)
82(12) % Rh5					
$Pr_{16}Rh_{9.55(9)}In_{1.45(9)}$					
Pr1	16*l*	0.08013(5)	0.20431(5)	0.30982(6)	154(1)
Pr2	8*i*	0.20888(8)	0.07466(8)	0	237(2)
Pr3	4*h*	0.14550(7)	$x+1/2$	1/2	158(2)
Pr4	4*f*	0	1/2	0.21109(12)	172(2)
Rh1	8*k*	0.17813(7)	$x+1/2$	0.22420(12)	205(3)
Rh2	4*h*	0.60239(11)	$x+1/2$	1/2	195(4)
Rh3	4*e*	0	0	0.15688(18)	179(3)
46(8) % In1	4*g*	0.65800(13)	$x+1/2$	0	212(6)
54(8) % Rh4					
50(10) % In2	2*b*	0	0	1/2	168(8)
50(10) % Rh5					
$Nd_{16}Rh_{9.61(7)}In_{1.39(7)}$					
Nd1	16*l*	0.07988(4)	0.20316(4)	0.31154(4)	145(1)
Nd2	8*i*	0.21062(6)	0.07309(7)	0	244(2)
Nd3	4*h*	0.14414(5)	$x+1/2$	1/2	142(2)
Nd4	4*f*	0	1/2	0.20647(9)	163(2)
Rh1	8*k*	0.17783(6)	$x+1/2$	0.22433(10)	198(2)
Rh2	4*h*	0.60254(8)	$x+1/2$	1/2	173(3)
Rh3	4*e*	0	0	0.15593(14)	164(2)
47(6) % In1	4*g*	0.65841(9)	$x+1/2$	0	249(5)
53(6) % Rh4					
45(8) % In2	2*b*	0	0	1/2	156(6)
55(8) % Rh5					
$La_{16}Rh_8Sn_3$					
La1	16*l*	0.08591(8)	0.20212(8)	0.3075(1)	143(2)
La2	8*i*	0.21069(12)	0.07555(12)	0	125(3)
La3	4*h*	0.13733(13)	$x+1/2$	1/2	172(5)
La4	4*f*	0	1/2	0.2123(2)	154(4)
Rh1	8*k*	0.17334(11)	$x+1/2$	0.22787(19)	184(4)
Rh2	4*h*	0.61390(19)	$x+1/2$	1/2	239(7)
Rh3	4*e*	0	0	0.1540(3)	205(6)
Sn1	4*g*	0.65585(13)	$x+1/2$	0	126(5)
Sn2	2*b*	0	0	1/2	217(9)

Table 4. (continued).

Atom	Wyckoff site	x	y	z	U_{eq}
$Pr_{16}Rh_{9.38(10)}Sn_{1.62(10)}$					
Pr1	16*l*	0.08010(7)	0.20212(7)	0.31172(9)	142(2)
Pr2	8*i*	0.20923(11)	0.07501(10)	0	157(3)
Pr3	4*h*	0.14463(11)	$x+1/2$	1/2	158(4)
Pr4	4*f*	0	1/2	0.21607(18)	153(3)
Rh1	8*k*	0.17731(11)	$x+1/2$	0.22661(18)	182(4)
Rh2	4*h*	0.60542(17)	$x+1/2$	1/2	198(5)
Rh3	4*e*	0	0	0.1557(2)	147(5)
53(9) % Sn1	4*g*	0.65678(14)	$x+1/2$	0	166(8)
47(9) % Rh4					
55(13) % Sn2	2*b*	0	0	1/2	178(11)
45(13) % Rh5					
$Pr_{16}Rh_{10.20(9)}Sb_{0.80(9)}$					
Pr1	16*l*	0.08086(8)	0.20035(8)	0.31257(11)	128(2)
Pr2	8*i*	0.21452(14)	0.07045(16)	0	211(4)
Pr3	4*h*	0.13947(14)	$x+1/2$	1/2	143(4)
Pr4	4*f*	0	1/2	0.1979(2)	164(4)
Rh1	8*k*	0.17363(14)	$x+1/2$	0.2269(2)	161(5)
Rh2	4*h*	0.6101(3)	$x+1/2$	1/2	210(8)
Rh3	4*e*	0	0	0.1522(4)	154(6)
32(9) % Sb1	4*g*	0.6575(2)	$x+1/2$	0	331(16)
68(9) % Rh4					
16(10) % Sb2	2*b*	0	0	1/2	174(16)
84(10) % Rh5					
$La_{16}Rh_{8.76(2)}Pb_{2.24(2)}$					
La1	16*l*	0.08518(8)	0.20072(8)	0.30894(9)	180(2)
La2	8*i*	0.20988(12)	0.07672(12)	0	150(3)
La3	4*h*	0.13838(13)	$x+1/2$	1/2	222(5)
La4	4*f*	0	1/2	0.21496(18)	171(4)
Rh1	8*k*	0.17249(11)	$x+1/2$	0.22868(17)	200(4)
Rh2	4*h*	0.6182(2)	$x+1/2$	1/2	339(8)
Rh3	4*e*	0	0	0.1509(3)	198(6)
89(1) % Pb1	4*g*	0.65389(8)	$x+1/2$	0	140(5)
11(1) % Rh4					
47(2) % Pb2	2*b*	0	0	1/2	191(10)
53(2) % Rh5					

cus on this stannide. In Fig. 2 we present a view of the $La_{16}Rh_8Sn_3$ structure along the *c* axis. The remarkable structural motif of this structure is the column of face-sharing square prisms and antiprisms, in which the smaller rhodium atoms fill the antiprisms. The stacking of these prismatic units is always one prism followed by two anti-prisms. All our structure refinements showed well behaved displacement parameters for the 2*b* sites within the square prisms. The U_{33} values were always close to or even slightly smaller than the U_{11} values. There was no need to introduce a split position 0 0 *z* instead of 0 0 1/2, as it was the case for $Ca_{16}Sb_{11}$ [10], $Eu_{16}Sb_{11}$, and $Eu_{16}Bi_{11}$ [18].

In order to facilitate comparison of the centrosymmetric $La_{16}Rh_8Sn_3$ and the non-centrosymmetric $Ca_{16}Sb_{11}$ structure, we present a group-subgroup

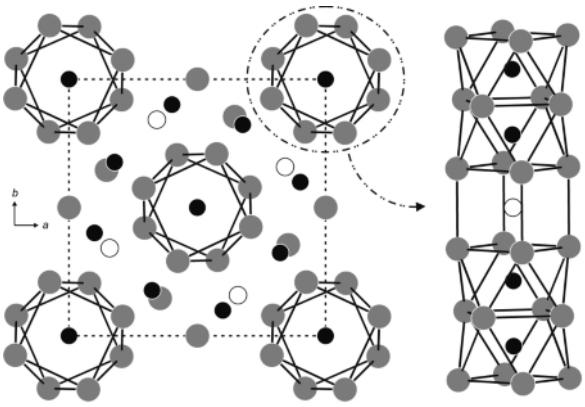

Fig. 2. The crystal structure of $La_{16}Rh_8Sn_3$. Lanthanum, rhodium, and tin atoms are drawn as medium grey, black filled, and open circles, respectively. For details see text.

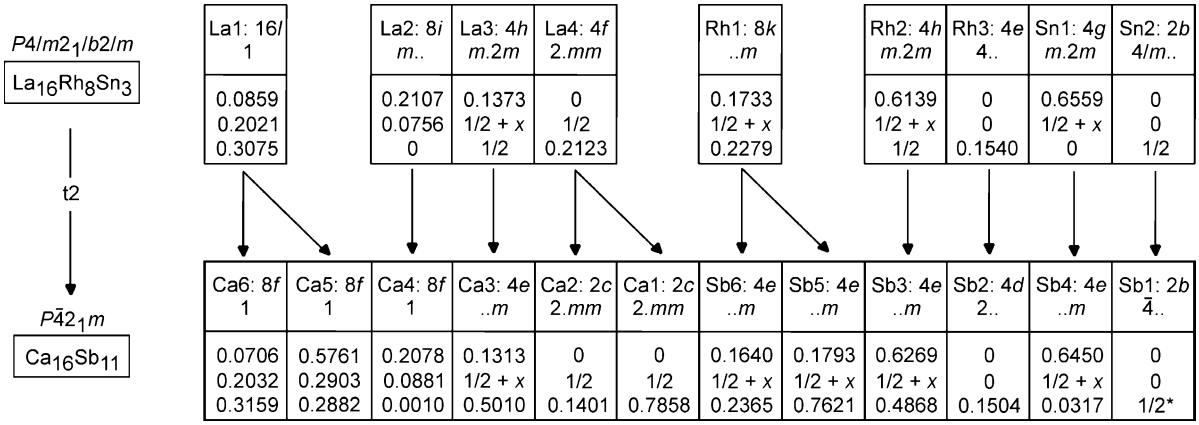

Fig. 3. Group-subgroup scheme in the Bärnighausen formalism [19 – 22] for the structures of $La_{16}Rh_8Sn_3$ and $Ca_{16}Sb_{11}$ [10]. The index for the *translationengleiche* (t) symmetry reduction and the evolution of the atomic parameters are given. Note, that the Sb1 site in $Ca_{16}Sb_{11}$ [10] was refined with a split position 0 0 0.4698 with 50 % occupancy.

Table 5. Interatomic distances (pm) in the structure of $La_{16}Rh_8Sn_3$. All distances within the first coordination spheres are listed. Standard deviations are all equal or smaller than 0.4 pm.

La1:	1	Rh2	297.8	La4:	2	Rh1	300.0
	1	Rh1	306.8		2	Sn1	342.8
	1	Rh3	309.1		2	Rh2	348.3
	1	Sn2	330.2		2	La3	372.7
	1	Rh1	360.3		4	La1	390.6
	1	Sn1	363.0	Rh1:	1	La3	278.9
	1	La2	365.2		2	La2	293.6
	1	La1	366.3		1	La4	300.0
	1	La2	376.2		2	La1	306.8
	2	La1	379.5		2	La1	360.3
	1	La1	384.6		1	Sn1	372.8
	1	La3	387.1	Rh2:	4	La1	297.8
	1	La4	390.6		2	La3	308.3
	1	La3	397.0		2	La4	348.3
La2:	2	Rh1	293.6		1	Rh2	393.7
	2	Rh3	313.8	Rh3:	1	Rh3	307.7
	1	Sn1	326.4		4	La1	309.1
	1	Sn1	335.0		4	La2	313.8
	2	La1	365.2		1	Sn2	345.6
	1	La2	369.4	Sn1:	2	La2	326.4
	2	La1	376.2		2	La2	335.0
	2	La2	386.8		2	La4	342.8
La3:	2	Rh1	278.9		4	La1	363.0
	2	Rh2	308.3		2	Rh1	372.8
	2	La4	372.7	Sn2:	8	La1	330.2
	4	La1	387.1		2	Rh3	345.6
	4	La1	397.0				

scheme in the Bärnighausen formalism [19 – 22] in Fig. 3. $Ca_{16}Sb_{11}$ crystallizes in space group $P\bar{4}2_1m$, a *translationengleiche* subgroup of $P4/mbm$. The evolution of the positional parameters in Fig. 3 shows a splitting for three sites. The deviations of the refined values from the subcell data are pronounced, enforcing the non-centrosymmetric structure. The striking difference between both structures concerns the chemical nature (antimony *vs*. rhodium) and size (141 pm covalent radius [23] for antimony *vs*. 125 pm for rhodium). This is most likely the reason for the lower symmetry of the $Ca_{16}Sb_{11}$ structure. In view of the split position for the 2*b* Sb1 site (refined with 50 % occupancy on 4*d* with $z = 0\ 0.4698$ [10]), the structural model in space group $P\bar{4}2_1m$ can only be considered as an average structure. The same holds true for $Eu_{16}Sb_{11}$ and $Eu_{16}Bi_{11}$ [18]. An ordering of the split positions would be possible in space group $P\bar{4}$, a *translationengleiche* subgroup of index 2 of $P\bar{4}2_1m$, where the 2*b* site splits into two distinct sites 1*b* and 1*d*. Low-temperature investigations for this structure type are under way in order to search for a possible superstructure formation.

The shortest distance in the $La_{16}Rh_8Sn_3$ structure occurs for Rh1–La3 (279 pm). All three rhodium sites have such La–Rh contacts with Rh–La distances ranging from 279 to 314 pm. Most of these distances are even smaller than the sum of the covalent radii [23] of 294 pm, indicating substantial Rh–La bonding. This is in line with the course of the electronegativities (2.28 for Rh and 1.10 for La on the Pauling scale [23]). The Sn2 atoms within the square prisms have Sn2–La1 distances of 330 pm, slightly longer than the sum of the covalent radii [23] of 309 pm. As a consequence of the high lanthanum content, within the $La_{16}Rh_8Sn_3$ structure we observe no di-

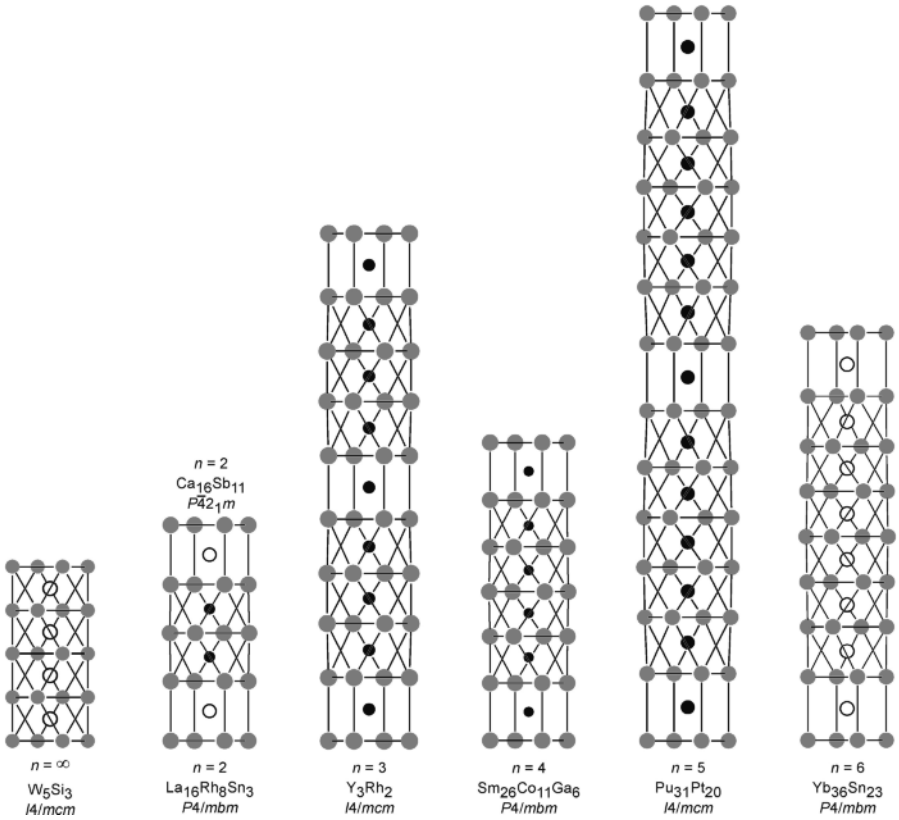

Fig. 4. Comparison of the columns of face-sharing tetragonal prisms and antiprisms in diverse structure types of the series $A_{5n+6}B_{3n+5}$. For details see text.

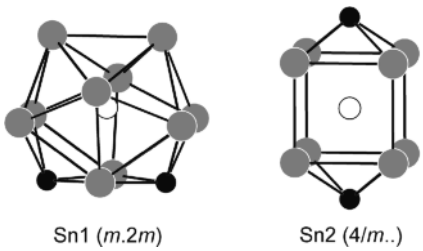

Fig. 5. Coordination of the two crystallographically independent tin sites in $La_{16}Rh_8Sn_3$. Lanthanum, rhodium, and tin atoms are drawn as medium grey, black filled, and open circles, respectively. The site symmetries are indicated.

rect Rh–Sn contacts. The shortest Rh–Sn distance of 346 pm is much longer than the sum of the covalent radii of 265 pm. In the structures of LaRhSn [24], $LaRhSn_2$ [25], or $CaRhSn_2$ [26], the rhodium and tin atoms build up three-dimensional [RhSn] and [$RhSn_2$] networks in which the cations fill larger cavities. In those stannides the Rh–Sn distances are the shortest ones.

Between adjacent square anti-prisms we observe Rh3–Rh3 distances of 308 pm. The latter are significantly longer than in *fcc* rhodium (269 pm) [27] and can not be considered as bonding. They are just a consequence of the anti-prismatic arrangement. The various La–La distances within the first coordination spheres of the four crystallographically independent lanthanum sites range from 365 to 397 pm, comparable to *fcc* lanthanum (375 pm) [27].

The structure of $La_{16}Rh_8Sn_3$ is a further member of Parthé's series of $A_{5n+6}B_{3n+5}$ structures [11]. $La_{16}Rh_8Sn_3$ is the centrosymmetric $n = 2$ member. The other members are W_5Si_3 ($n = \infty$) [28], $Ca_{16}Sb_{11}$ ($n = 2$) [10], Y_3Rh_2 ($n = 3$) [11, 29], $Sm_{26}Co_{11}Ga_6$ ($n = 4$) [30], $Pu_{31}Pt_{20}$ ($n = 5$) [31], and $Yb_{36}Sn_{23}$ ($n = 6$) [32]. Similar to the pair $Ca_{16}Sb_{11}$ and $La_{16}Rh_8Sn_3$ for $n = 2$, also $Pu_{31}Pt_{20}$ with $n = 5$ has a *p* element counterpart $Ca_{31}Sn_{20}$ [33]. The different columns which occur in the $A_{5n+6}B_{3n+5}$ structures are presented in Fig. 4, the corresponding crystallographic data are listed in Table 6. The members with even *n* crystal-

Table 6. Structure types within the homologous series $A_{5n+6}B_{3n+5}$.

Structure	n	a (pm)	c (pm)	Space group	Reference
W_5Si_3	∞	964.5	497.0	$I4/mcm$	[28]
$Ca_{16}Sb_{11}$	2	1225.3(3)	1131.3(4)	$P\bar{4}2_1m$	[10]
$La_{16}Rh_8Sn_3$	2	1220.7(1)	997.9(2)	$P4/mbm$	This work
$Y_{21}Rh_{14}$ (Y_3Rh_2)	3	1123.2(2)	2516(1)	$I4/mcm$	[11, 29]
$Sm_{26}Co_{11}Ga_6$	4	1171.3(4)	1517.1(7)	$P4/mbm$	[30]
$Pu_{31}Pt_{20}$	5	1130.2(5)	3738.8(2)	$I4/mcm$	[31]
$Yb_{36}Sn_{23}$	6	1238.69(5)	2293.5(1)	$P4/mbm$	[32]

lize with a primitive ($P4/mbm$), those with an odd n with a body-centered ($I4/mcm$) tetragonal space group. The columns are arranged in the form of tetragonal rod packings. In the binary compounds the square prisms and anti-prisms are filled either by the transition metal or by the p element. In the structure of $La_{16}Rh_8Sn_3$ we observed an ordering within the two prism types. Detailed substitution experiments have recently been carried out for various solid solutions $RE_3T_{2-x}In_x$ [34]. These ternary $n = 3$ members show different ordering patterns within the prisms.

Finally we draw back to the tin coordination. The near-neighbor environments of the two crystallographically independent tin sites in $La_{16}Rh_8Sn_3$ are shown in Fig. 5. The Sn1 and Sn2 atoms have 10, respectively 8 lanthanum neighbors with two additional rhodium neighbors at longer Rh–Sn distances capping rectangular faces. These different coordinations lead to different site symmetries, *i. e.* $m.2m$ for Sn1 and $4/m..$ for Sn2 as discussed in more detail below.

Mössbauer spectroscopic characterization

Fig. 6 displays the ^{119}Sn Mössbauer spectra of the $La_{16}Rh_8Sn_3$ and $Pr_{16}Rh_9Sn_2$ samples at 77 K together with transmission integral fits. The corresponding fitting parameters are listed in Table 7. Both spectra could be well reproduced with a superposition of two signals in the ratio of 2 : 1 with almost similar isomer shifts, but distinctly different quadrupole splitting parameters. In agreement with the lower site symmetry, the signal with the higher quadrupole splitting parameter was assigned to the Sn1 sites. A similar behavior was observed for YbAgSn [35]. The experimentally observed isomer shifts indicated considerable s elelctron density at the tin nuclei [36]. Based on this result we can conclude that there is charge transfer from lanthanum not only to the electronegative rhodium, but also to the tin atoms. This is similar to $LaRhSn_2$ [25], while in other equiatomic RERhSn stannides [37] the isomer shifts are slightly smaller.

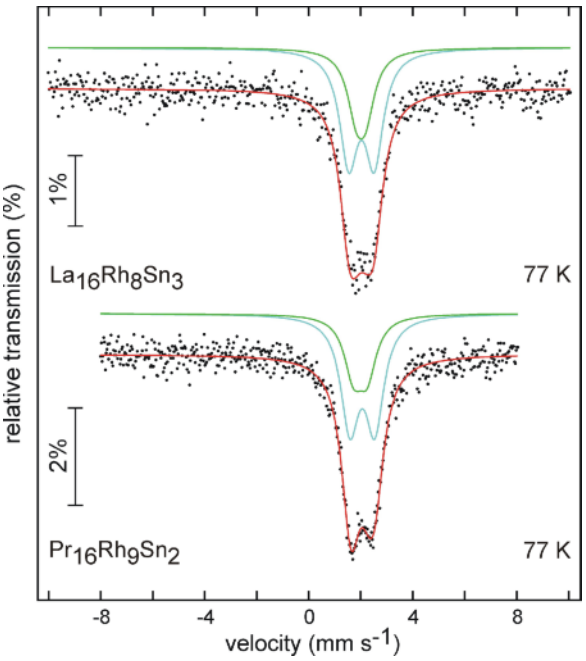

Fig. 6 (color online). Experimental and simulated ^{119}Sn Mössbauer spectra of $La_{16}Rh_8Sn_3$ and $Pr_{16}Rh_9Sn_2$ at 77 K.

Table 7. Fitting parameters of ^{119}Sn and ^{121}Sb Mössbauer spectroscopic measurements of $La_{16}Rh_8Sn_3$, $Pr_{16}Rh_9Sn_2$ and $Pr_{16}Rh_9Sb_2$. Numbers in parentheses represent the statistical errors in the last digit. (δ), isomer shift; (Δ), experimental line width; (ΔE_Q), electric quadrupole splitting. The site assignments and site symmetries are indicated.

Compound	Site	δ (mm s^{-1})	ΔE_Q (mm s^{-1})	Γ (mm s^{-1})
$La_{16}Rh_8Sn_3$	Sn1 ($m.2m$)	2.03(1)	0.98(2)	0.85[a]
	Sn2 ($4/m..$)	2.01(2)	0.36(6)	0.85[a]
$Pr_{16}Rh_9Sn_2$	Sn1 ($m.2m$)	2.06(1)	0.96(2)	0.85[a]
	Sn2 ($4/m..$)	1.97(3)	0.53(5)	0.85[a]
$Pr_{16}Rh_9Sb_2$	Sb1/Sb2	−8.22(3)	0[a]	2.8(1)

[a] Parameter fixed during the fitting procedure.

The ^{121}Sb spectrum of $Pr_{16}Rh_9Sb_2$ is presented in Fig. 7. The much higher natural line width of antimony

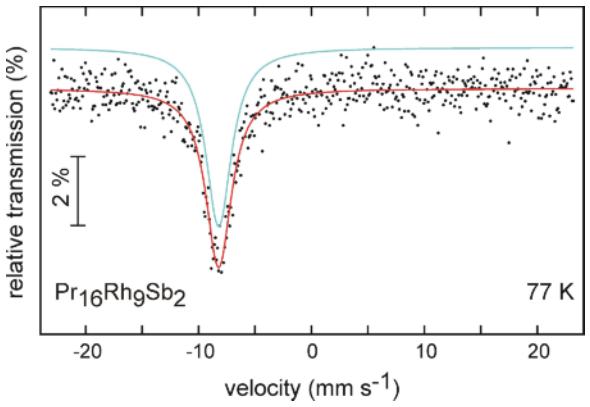

Fig. 7 (color online). Experimental and simulated ^{121}Sb Mössbauer spectrum of $Pr_{16}Rh_9Sb_2$ at 77 K.

excludes high resolution of the spectrum and an independent refinement of the quadrupole splitting parameter and the experimental line width was not possible. Although the structure refinement also showed two Wyckoff sites with Rh/Sb mixing, only the superimposed signal of both spectral contributions could be observed. The isomer shift of -8.22 mm s^{-1} points to an antimonide character [38], similar to the series Yb*T*Sb [39] and *RE*ZnSbO [40].

Acknowledgement

We thank Dipl.-Ing. U. Ch. Rodewald for the intensity data collections. This work was financially supported by the Deutsche Forschungsgemeinschaft.

[1] A. Palenzona, F. Canepa, P. Manfrinetti, *J. Alloys Compd.* **1993**, *194*, 63.
[2] A. Raman, *J. Less-Common Met.* **1972**, *26*, 199.
[3] A. Raman, *J. Less-Common Met.* **1976**, *48*, 111.
[4] A. E. Dwight, R. A. Conner Jr., J. W. Downey, *Acta Crystallogr.* **1965**, *18*, 835.
[5] F. Stadler, Th. Fickenscher, R. Pöttgen, *Z. Naturforsch.* **2001**, *56b*, 1241.
[6] F. Tappe, U. Ch. Rodewald, R.-D. Hoffmann, R. Pöttgen, *Z. Naturforsch.* **2011**, *66b*, 559.
[7] F. M. Schappacher, R. Pöttgen, *Monatsh. Chem.* **2008**, *139*, 1137.
[8] F. Tappe, R. Pöttgen, *Z. Naturforsch.* **2009**, *64b*, 184.
[9] F. Tappe, R. Pöttgen, *Rev. Inorg. Chem.* **2011**, *31*, 5.
[10] E. A. Leon-Escamilla, W.-M. Hurng, E. S. Peterson, J. D. Corbett, *Inorg. Chem.* **1997**, *36*, 703.
[11] J. Le Roy, J. M. Moreau, D. Paccard, E. Parthé, *J. Less-Common Met.* **1980**, *76*, 131.
[12] R. Pöttgen, Th. Gulden, A. Simon, *GIT Labor-Fachzeitschrift* **1999**, *43*, 133.
[13] R. Pöttgen, A. Lang, R.-D. Hoffmann, B. Künnen, G. Kotzyba, R. Müllmann, B. D. Mosel, C. Rosenhahn, *Z. Kristallogr.* **1999**, *214*, 143.
[14] K. Yvon, W. Jeitschko, E. Parthé, LAZY PULVERIX, A Computer Program for Calculating X-ray and Neutron Diffraction Powder Patterns, University of Geneva, Geneva (Switzerland) **1977**. See also: K. Yvon, W. Jeitschko, E. Parthé, *J. Appl. Crystallogr.* **1977**, *10*, 73.
[15] G. M. Sheldrick, SHELXS-97, Program for the Solution of Crystal Structures, University of Göttingen, Göttingen (Germany) **1997**. See also: G. M. Sheldrick, *Acta Crystallogr.* **1990**, *A46*, 467.
[16] G. M. Sheldrick, SHELXL-97, Program for the Refinement of Crystal Structures, University of Göttingen, Göttingen (Germany) **1997**. See also: G. M. Sheldrick, *Acta Crystallogr.* **2008**, *A64*, 112.
[17] A. Palenzona, *J. Alloys Compd.* **1992**, *190*, 13.
[18] J. Y. Chan, M. M. Olmstead, H. Hope, S. M. Kauzlarich, *J. Solid State Chem.* **2000**, *155*, 168.
[19] H. Bärnighausen, *Commun. Math. Chem.* **1980**, *9*, 139.
[20] U. Müller, *Z. Anorg. Allg. Chem.* **2004**, *630*, 1519.
[21] U. Müller in *International Tables for Crystallography*, Vol. A1, *Symmetry relations between space groups*, (Eds.: H. Wondratschek, U. Müller). 2nd Ed., John Wiley, Chichester, **2010**, pp. 44 – 56.
[22] U. Müller, *Symmetriebeziehungen zwischen verwandten Kristallstrukturen*, Vieweg + Teubner Verlag, Wiesbaden **2012**.
[23] J. Emsley, *The Elements*, Oxford University Press, Oxford **1999**.
[24] T. Schmidt, D. Johrendt, C. P. Sebastian, R. Pöttgen, K. Łątka, R. Kmieć, *Z. Naturforsch.* **2005**, *60b*, 1036.
[25] D. Niepmann, R. Pöttgen, B. Künnen, G. Kotzyba, C. Rosenhahn, B. D. Mosel, *Chem. Mater.* **1999**, *11*, 1597.
[26] R.-D. Hoffmann, D. Kußmann, U.Ch. Rodewald, R. Pöttgen, C. Rosenhahn, B. D. Mosel, *Z. Naturforsch.* **1999**, *54b*, 709.
[27] J. Donohue, *The Structures of the Elements*, Wiley, New York (USA) **1974**.
[28] B. Aronsson, *Acta Chem. Scand.* **1955**, *9*, 1107.
[29] J.-M. Moreau, D. Paccard, E. Parthé, *Acta Crystallogr.* **1976**, *B32*, 1767.
[30] Ya. P. Yarmolyuk, Yu. N. Grin', O. M. Olesh, *Sov. Phys. Crystallogr.* **1980**, *25*, 143.

[31] D. T. Cromer, A. C. Larson, *Acta Crystallogr.* **1977**, *B33*, 2620.
[32] E. A. Leon-Escamilla, J. D. Corbett, *Inorg. Chem.* **1999**, *38*, 738.
[33] M. L. Fornasini, E. Franceschi, *Acta Crystallogr.* **1977**, *B33*, 3476.
[34] R. Zaremba, U. Ch. Rodewald, V. I. Zaremba, R. Pöttgen, *Z. Naturforsch.* **2007**, *62b*, 1397.
[35] R. Pöttgen, P. E. Arpe, C. Felser, D. Kußmann, R. Müllmann, B. D. Mosel, B. Künnen, G. Kotzyba, *J. Solid State Chem.* **1999**, *145*, 668.
[36] P. E. Lippens, *Phys. Rev. B* **1999**, *60*, 4576.
[37] R. Mishra, R. Pöttgen, R.-D. Hoffmann, H. Trill, B. D. Mosel, H. Piotrowski, M. F. Zumdick, *Z. Naturforsch.* **2001**, *56b*, 589.
[38] P. E. Lippens, *Solid Sate Commun.* **2000**, *113*, 399.
[39] R. Mishra, R. Pöttgen, R.-D. Hoffmann, Th. Fickenscher, M. Eschen, H. Trill, B. D. Mosel, *Z. Naturforsch.* **2002**, *57b*, 1215.
[40] I. Schellenberg, H. Lincke, W. Hermes, V. Dittrich, R. Glaum, M. H. Möller, R. Pöttgen, *Z. Naturforsch.* **2010**, *65b*, 1191.